First-order differential equations for single-particle quantum mechanical systems

Daniel Gebremedhin [*] and Charles Weatherford [†]

Physics Department, Florida A&M University, Tallahassee, Florida 32307, USA

Coupled first-order differential forms of a single-particle Schrödinger equation are presented. These equations are convenient to solve efficiently using the widely available ordinary differential equation solvers. This is particularly true because the solutions to the differential equation are two sets of complementary functions that share simple and consistent mathematical relationships at the boundary and across the domain for a given potential. The differential equations are derived from an integral equation obtained using the Green's function for the kinetic operator, making them universally applicable to various systems. These equations are applied to the Yukawa potential $-e^{-\alpha r}/r$ to calculate the critical screening parameter $\alpha = 1.190\,612\,421\,060\,617\,705\,342\,777\,106\,361\,05$ using a standard quadruple precision calculation, which is the most accurate compared to similar calculations in the past that confirm the first 30 significant figures. Also reported is the interesting coincident point with the eigenvalue, $\alpha = -E = 0.274\,376\,862\,689\,408\,994\,894\,705\,268\,554\,458$.

I. INTRODUCTION

Electronic structure calculations are mostly done by solving a single-particle equation thanks to density functional theory or Hartree-Fock theory that have made the otherwise complicated many-body physics manageable [1,2]. Further simplifications that arise from symmetry consideration or other approximations within the theory lead to a second-order differential equation (DE) that can be directly integrated. The resulting solutions obtained this way are more efficient than those obtained from a diagonalization method because they avoid basis set optimization or dealing with large eigensystems—processes associated with applying the variational principle. But since integration is not second order by nature, it is necessary to cast the equations into a first-order form to make maximum use of available ordinary DE solvers. Despite its frequent use, only a little thought is given to this procedure other than simultaneously solving for the function and its first derivative.

This article revisits this necessary procedure of transforming a single-particle time-independent Schrödinger equation into a set of first-order DEs [3,4] by presenting an *ab initio* derivation. The derivation utilizes the Green's function for the kinetic operator, which makes it universally applicable to systems with different potentials. A spherical coordinate system, which is the most popular coordinate system in electronic structure calculations, is used. The derivations shown here can be easily implemented in a different coordinate system and/or Green's function. The

resulting DEs are not only versatile but also aesthetically appealing.

The spherically symmetric version of the equations is applied later to the Yukawa and related screened Coulomb potentials. These screened potentials have relevance in numerous physical applications. However, only their numerical aspects are considered here [5–7]. For $\alpha = 0$, the system with the potential $-e^{-\alpha r}/r$ is identical to a hydrogen atom. But as α increases, the electron becomes less tightly bound, and after some critical value of the parameter, it can no longer retain a bound state. The potentials' screening parameter and eigenvalue pair (α, E) have been successfully calculated and reported previously, but not near the critical values, especially as E increases towards the continuum. Only a few digits of the critical value of α were calculated until recently [8,9]. Its electronic density at the origin [10] is another quantity that becomes numerically challenging to compute near the critical values. The derived DE is implemented to produce a comprehensive table of benchmark values for a wide range of these quantities.

II. INTEGRAL EQUATION

The nonrelativistic, time-independent Schrödinger equation for a one-particle quantum mechanical system is (atomic units will be used throughout)

$$\left(-\tfrac{1}{2}\nabla_{\mathbf{r}}^2 + V(\mathbf{r}) - E\right)\Psi(\mathbf{r}) = 0, \qquad (1)$$

where V and E are the total potential and energy of the system, respectively. The notation $r \equiv |\mathbf{r}|$ and $\hat{r} \equiv \mathbf{r}/r$ are used for a position vector $\mathbf{r}$ in three-dimensional coordinate space. Using the Green's function for the Laplace operator given by $\nabla_{\mathbf{r}}^2 [(-4\pi |\mathbf{r} - \mathbf{x}|)^{-1}] = \delta(\mathbf{r} - \mathbf{x})$ [11], the solution can be formally written

_____

[*]daniel1.gebremedhin@famu.edu

[†]charles.weatherford@famu.edu

as

$$\Psi(\mathbf{r}) = \sum_L \frac{2}{2l+1} Y_L(\hat{r}) \int Y_L{}^*(\hat{x}) \frac{r_<^l}{r_>^{l+1}} [E - V(\mathbf{x})] \Psi(\mathbf{x}) d^3x, \tag{2}$$

where the Laplace expansion of $|\mathbf{r} - \mathbf{x}|^{-1}$ in the spherical coordinate system has been employed. Here, $L \equiv \{l, m\}$ is a composite index, Y is a spherical harmonic function, and the $>$ and $<$ signify the greater and lesser of r and x, respectively. The above equation is itself an expansion in terms of Y given below:

$$\Psi(\mathbf{r}) = \sum_L \psi_L(r) Y_L(\hat{r}) \equiv \sum_{l=0}^{\infty} \sum_{m=-l}^{l} \psi_l^m(r) Y_l^m(\hat{r}), \tag{3}$$

where

$$\psi_L(r) = \frac{2}{2l+1} \int Y_L^*(\hat{x}) \frac{r_<^l}{r_>^{l+1}} [E - V(\mathbf{x})] \Psi(\mathbf{x}) d^3x. \tag{4}$$

Substituting Eq. (3) on the right-hand side of the above equation, one can write

$$\psi_L(r) = \sum_{L'} \int_0^{\infty} x \frac{r_<^l}{r_>^{l+1}} P_{LL'}(x) \psi_{L'}(x) dx, \tag{5}$$

where P is a symmetric matrix of double integrals over the angular variables that incorporate all of the physics of the system.

$$P_{LL'}(r) = \frac{2r}{2l+1} \int Y_L{}^*(\hat{r}) [E - V(\mathbf{r})] Y_{L'}(\hat{r}) d\hat{r}. \tag{6}$$

The factor r up front helps to regularize the singularity in Coulomb-like ($\propto 1/r$) potentials. Now, let us break the x axis into two parts as $[0, r]$ and $[r, \infty)$ and write Eq. (5) more explicitly as

$$\psi_L(r) = \sum_{L'} \left[\frac{1}{r^{l+1}} \int_0^r x^{l+1} P_{LL'}(x) \psi_{L'}(x) dx + r^l \right.$$
$$\left. \times \int_r^{\infty} x^{-l} P_{LL'}(x) \psi_{L'}(x) dx \right]. \tag{7}$$

The right-hand side of the above equation has a striking similarity with the potential in Poisson's equation if the radial part of the density replaces the product $P\psi$ [12].

III. COUPLED FIRST-ORDER DIFFERENTIAL EQUATIONS

To get the desired DEs, first write the above integral equation in the following form:

$$\psi_L(r) = \frac{1}{r^{l+1}} S_L(r) + r^l C_L(r), \tag{8}$$

where

$$S_L(r) = \sum_{L'} \int_0^r dx \, x^{l+1} P_{LL'}(x) \psi_{L'}(x), \tag{9}$$

$$C_L(r) = \sum_{L'} \int_r^{\infty} dx \, x^{-l} P_{LL'}(x) \psi_{L'}(x). \tag{10}$$

For reasons that will soon be clear, the above two complementary functions shall be named S (ine) and C (osine) component functions, respectively. Taking a derivative (denoted below by an overhead dot) of the above equations with respect to r gives

$$\dot{S}_L(r) = \sum_{L'} r^{l+1} P_{LL'}(r) \psi_{L'}(r), \tag{11}$$

$$\dot{C}_L(r) = -\sum_{L'} r^{-l} P_{LL'}(r) \psi_{L'}(r). \tag{12}$$

Clearly, $\dot{S}_L(r) = -r^{2l+1} \dot{C}_L(r)$. This is the defining relationship that keeps the numerical behavior of $\dot{S}$ and $\dot{C}$ universally simple and consistent. They become equal in magnitude only at $r = 1$. For $r > 1$, $|\dot{S}| > |\dot{C}|$, and vice versa for $r < 1$. This is also a marked qualitative difference from the traditional $(\psi, \dot{\psi})$ pair, whose mutual relationship depends on the potential V.

Substituting for ψ from Eq. (8), and after some rearrangement, results in the following first-order, homogeneous matrix DE:

$$\begin{bmatrix} \dot{S}_L(r) \\ \dot{C}_L(r) \end{bmatrix} = \sum_{L'} P_{LL'}(r) \begin{bmatrix} r^{l-l'} & r^{l+l'+1} \\ -r^{-l-l'-1} & -r^{l'-l} \end{bmatrix} \begin{bmatrix} S_{L'}(r) \\ C_{L'}(r) \end{bmatrix}. \tag{13}$$

P completely factors out of the above 2×2 kernel matrix. The eigenvalues of this matrix are $(0, r^{l-l'} - r^{l'-l})$, which prohibits the possibility of using the powerful spectral decomposition theorem [13] to further decouple Eq. (13) into two sets of DEs. The exact implications of these eigenvalues are not clear, but the overall effect seems to be consistent with the fact that the solutions are essentially "decoupled" into small and big components. The overall result according to our numerical tests on electronic structure calculations is that Eq. (13) can be integrated in a very stable manner out to large distances where the wavefunction is well decayed. Its familiar form also makes it convenient to integrate using readily available DE solvers as long as the summation over L' is finite. Construction of this linear, first-order DE boils down to an evaluation of P. From Eqs. (9) and (10), by definition, the S and C functions vanish at the origin and at infinity, respectively. Thus, one of the key advantages of these functions is that, for all potentials, the integration can proceed outwards with the initial condition $(S_L(0), C_L(0)) = (0, 1)$ and the corresponding ψ renormalized properly afterward.

Thus, one can, in principle, solve the above equation and generate the basis functions that belong to the same given energy E and construct the solution using Eq. (3). The size of the matrix DE in Eq. (13) is subjective to the (spherical) symmetry of the potential or how convergent the total wavefunction Ψ is in representing with the spherical harmonics basis set. Next, we will take a closer look at the simple but important spherically symmetric case of $V(\mathbf{r}) \to V(r)$ and use it to describe the numerical advantages that this form of the equations portend and, in the process, lay out some insight for working with the full potential.
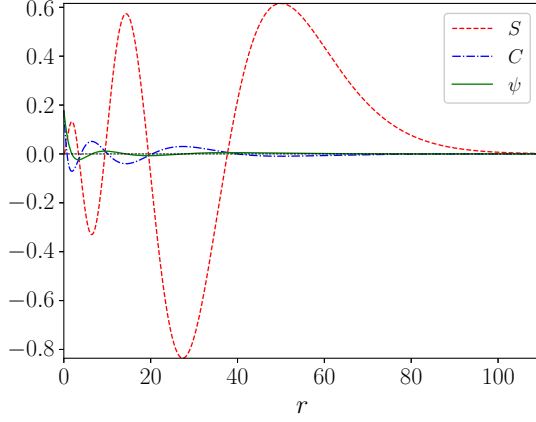
FIG. 1. The 5s eigenstate ψ of hydrogen atom and the corresponding S and C functions. The S function is overall more prominent than C.

A. Radial equation

Due to the orthonormality of the spherical harmonics, for a radial potential Eq. (6) reduces to

$$P_l(r) = \frac{2r}{2l+1}[E - V(r)], \quad \forall m, -l \leqslant m \leqslant l, \quad (14)$$

where the magnetic quantum number m is suppressed to avoid clutter. And hence, Eq. (13) becomes

$$\begin{bmatrix} \dot{S}_l(r) \\ \dot{C}_l(r) \end{bmatrix} = P_l(r) \begin{bmatrix} 1 & r^{2l+1} \\ -r^{-2l-1} & -1 \end{bmatrix} \begin{bmatrix} S_l(r) \\ C_l(r) \end{bmatrix}. \quad (15)$$

They are exponential in nature near and far from the origin: namely, for short range $S_l(r) \approx e^{P_l(r)}$, and for long range $C_l(r) \approx e^{-P_l(r)}$. Their typical plot shown in Fig. 1 indicates that they evolve into big and small components in such a way that, according to our tests, is also numerically conducive. Both eigenvalues of the above 2×2 matrix vanish, which again renders the two equations inseparable. However, by going into a phase-amplitude representation of the S and C functions, it is possible to obtain two decoupled equations, which allows for an alternative and interesting path towards the solution.

B. Phase-amplitude representation

In addition to their values at the origin and the simple relationship between their derivatives, a typical overlay plot of both the S and C functions, as shown in Fig. 1, makes it apparent that they resemble the trigonometric sin and cos functions. This warrants investigation for an alternate form of Eq. (15) that best approximates this peculiar behavior for further pedagogical or computational benefits. To this end, let us represent the two functions with the following phase-amplitude *ansatz*.

$$S_l(r) = A_l(r) \sin[\Phi_l(r)], \quad C_l(r) = A_l(r) \cos[\Phi_l(r)], \quad (16)$$

with inverse relations,

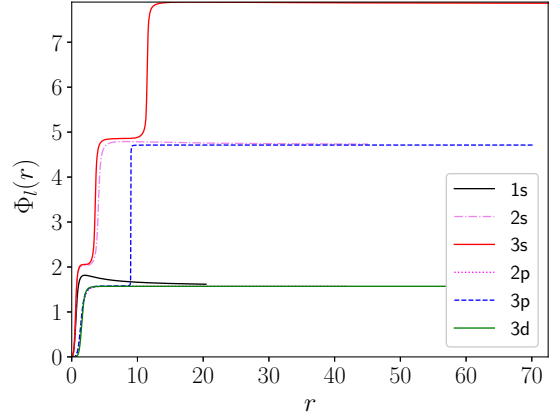$$A_l(r) = \sqrt{S_l^2(r) + C_l^2(r)}, \quad \Phi_l(r) = \tan^{-1}\left[\frac{S_l(r)}{C_l(r)}\right], \quad (17)$$

FIG. 2. The phase function Φ for the first few states of a hydrogen atom.

and hence, their name. After carrying out the derivatives, substituting into Eq. (15), and solving the resulting simultaneous equations, it can be shown that Φ and A obey the following two DEs:

$$\dot{\Phi}_l(r) = P_l(r)(r^{l+1/2} \cos[\Phi_l(r)] + r^{-l-1/2} \sin[\Phi_l(r)])^2, \quad (18)$$

$$\dot{A}_l(r) = P_l(r)\left(\frac{1}{2}(r^{2l+1} - r^{-2l-1}) \times \sin[2\Phi_l(r)] - \cos[2\Phi_l(r)]\right)A_l(r), \quad (19)$$

with $\Phi_l(0) = 0$ and $A_l(0) = |C_l(0)|$. Notice that once Eq. (18) is solved, the solution Φ becomes part of the potential for A in Eq. (19), which is a homogeneous, linear equation. Hence, one can solve Eqs. (18) and (19) separately, in that order, using two different methods chosen properly. For example, since A is always positive, one can opt to solve for $\ln A$ instead, which turns the problem into quadrature.

$$\ln A_l(r) = \ln|C_l(0)| + \int_0^r P_l(x)\left(\frac{1}{2}(x^{2l+1} - x^{-2l-1}) \times \sin[2\Phi_l(x)] - \cos[2\Phi_l(x)]\right)dx. \quad (20)$$

The price to pay for having such decoupled DEs is, of course, Eq. (18) is nonlinear. As shown in Fig. 2, its solution Φ is typically a monotonic function with a staircase like shape, which is slowly varying except near the roots of the wavefunction, where it jumps by an amount of what looks like an integral multiple of $\pi/2$. This shape around the roots is reminiscent of the arctan function around the origin. Thus, DE solvers implementing adaptive step sizes [14] are necessary for Eq. (18), especially for solutions with multiple roots. The phase-amplitude method is commonly used with the regular and irregular solutions of the continuum states, leading to a second-order, nonlinear DE for the amplitude referred to as the Milne DE [15,16], the details of which mirror an interesting compare and contrast with this section's content.

In passing, it is worth mentioning that Eq. (5) implies the following Green's function is available for the radial kinetic

TABLE I. The calculated results of the screening parameter α, ground state energy E_0, and the value of the wavefunction at the origin C_0 for the SCP potential. Values in square brackets are powers of 10. The critical value reported in [9] is $\alpha = 1.190\,612\,421\,060\,617\,705\,342\,777\,106\,362 \pm [-30]$.

α	E	$C_0(0)$
1.0[−33]	−0.499 999 999 999 999 999 999 999 999 999	1.999 999 999 999 999 999 999 999 999 9(9)
1.0[−32]	−0.499 999 999 999 999 999 999 999 999 991	1.999 999 999 999 999 999 999 999 999 9(1)
1.0[−31]	−0.499 999 999 999 999 999 999 999 999 900	1.999 999 999 999 999 999 999 999 999 9(6)
1.0[−30]	−0.499 999 999 999 999 999 999 999 999 000	2.000 000 000 000 000 000 000 000 000 0(1)
1.0[−20]	−0.499 999 999 999 999 999 990 000 000 000	1.999 999 999 999 999 999 999 999 999 9(6)
1.0[−10]	−0.499 999 999 900 000 000 007 499 999 999 500	1.999 999 999 999 999 985 000 000 00(2)
1.0[−1]	−0.407 058 030 613 403 156 754 507 070 361 108	1.986 502 278 187 072 206 286 886 166 677(5)[a]
1.0	−1.028 578 999 001 769 680 477 421 531 491 551[−2]	0.963 915 192 038 500 879 024 076 250 344(8)[b]

α	E	$C_0(0)$
0.274 376 862 689 408 994 894 705 268 554 458	−α	1.910 744 144 491 456 232 442 021 186 822(6)
0.616 395 604 379 678 530 676 311 513 164 471	−1.0[−1]	1.607 850 764 114 054 523 212 072 599 033 3(7)
1.190 593 340 822 933 007 093 495 100 956 29	−1.0[−10]	9.767 089 774 113 679 893 318 343 07(9)[−3]
1.190 612 420 869 815 050 957 096 818 781 82	−1.0[−20]	3.088 669 472 795 467 709 503 5(9)[−5]
1.190 612 421 060 615 797 316 233 221 804 34	−1.0[−30]	9.767 230 474 872 147 2(5)[−8]
1.190 612 421 060 617 705 323 696 840 922 20	−1.0[−40]	3.088 669 473 24(5)[−10]
1.190 612 421 060 617 705 342 776 915 558 39	−1.0[−50]	9.767 231 (2)[−13]
1.190 612 421 060 617 705 342 777 106 359 14	−1.0[−60]	3.1(8)[−15]
1.190 612 421 060 617 705 342 777 106 361 03	−1.0[−64]	3.0(1)[−16]
1.190 612 421 060 617 705 342 777 106 361 04	−1.0[−65]	2.2(7)[−16]
1.190 612 421 060 617 705 342 777 106 361 05	−1.0[−66]	(1)[−16]

[a]Reference value 1.986 502 278 2 from [10].
[b]Reference value 0.963 915 192 04 from [10].

operator.

$$\left[-\frac{1}{2}\frac{d^2}{dr^2} - \frac{1}{r}\frac{d}{dr} + \frac{l(l+1)}{2r^2} \right]\left(\frac{2}{2l+1}\frac{r_<^l}{r_>^{l+1}} \right) = \frac{1}{rx}\delta(r-x). \tag{21}$$

The techniques discussed in this article can be adopted to solve other second-order DEs with similar form.

IV. BOUND STATE EIGENVALUES

In this section, an algorithm for locating the eigenvalues of a DE that assumes little or no familiarity with the system is outlined. The algorithm relies on the fact that, upon the integration of the DEs outwards, only for the correct eigenvalue E does the wavefunction ψ decay exponentially to 0 [17]. For an eigenvalue that is just above or below the correct E, the corresponding ψ will eventually diverge, each with opposite sign. That is, if ψ for $E - \Delta E$ diverges towards $-\infty$, ψ for $E + \Delta E$ diverges towards $+\infty$ and vice versa. In practice, this phenomenon always occurs even for small ΔE, as long as we are working with finite precision because the irregular solutions of ψ will inevitably creep into the calculation and cause divergence. The algorithm exploits this extremely sensitive property of the orbitals to calculate E accurately.

This is done by monitoring the positive quantity $R(r) = \psi^2(r) + \dot\psi^2(r)$ and its minimum, say $R_{\min}$. The integration can be stopped when $R(r)/R_{\min}$ exceeds a prescribed large number (say, $\sim 10^4$), which is a reliable indicator that the solution is blasting off. The value of ψ at the end point can then be linked with an appropriate root-finding subroutine to

find the eigenvalues [18]. Once E is obtained, the portion of the solution beyond the location of $R_{\min}$ is to be discarded. Bracketing algorithms like the *bisection* method [4], that make use of the sign of the function to narrow down the bracketing interval, and thus are less susceptible to the smoothness of the function, would be preferable methods in this situation. As will be evident from the tables below, tolerances close to working precision can be afforded with this method. Another significant advantage of this algorithm is that one does not need to estimate the upper limit of the integration, unlike other methods that propagate in both forward and reverse directions and enforce continuity of the function and its slope somewhere in the middle [19].

V. EXAMPLE: SCREENED COULOMB POTENTIALS

As an example, we have employed Eqs. (18) and (20) [and alternately Eq. (15)] to calculate the ground state eigenstates of the Yukawa potential and its close relations shown below: namely, the Yukawa or static screened Coulomb potential (SCP), the exponential cosine screened Coulomb potential (ECSCP), and the Hulthén potential (HP):

$$V(r) = \begin{cases} -\dfrac{Ze^{-\alpha r}}{r} & \text{for SCP}, \\[2mm] \dfrac{e^{-\alpha r}}{(1+e^{-\alpha r})}\dfrac{Z\alpha}{\tanh(-\alpha r/2)} & \text{for HP}, \\[2mm] -\dfrac{Ze^{-\alpha r}}{r}\cos\alpha r & \text{for ECSCP}. \end{cases} \tag{22}$$

We shall closely follow the notation in [9], except for the equivalent formula in Eq. (22) for the HP potential, modified here for better numerical behavior, especially near the origin.

TABLE II. The calculated results of the screening parameter α, ground state energy E_0, and the value of the wavefunction at the origin C_0 for the ECSCP potential. Values in square brackets are powers of 10. The critical value reported in [9] is $\alpha =$ 0.720 524 085 881 953 095 871 917 136 919 $\pm [-30]$.

α	E	$C_0(0)$
1.0[−33]	−0.499 999 999 999 999 999 999 999 999 999	1.999 999 999 999 999 999 999 999 999 9(9)
1.0[−32]	−0.499 999 999 999 999 999 999 999 999 990	1.999 999 999 999 999 999 999 999 999 9(9)
1.0[−31]	−0.499 999 999 999 999 999 999 999 999 900	1.999 999 999 999 999 999 999 999 999 9(6)
1.0[−30]	−0.499 999 999 999 999 999 999 999 999 000	2.000 000 000 000 000 000 000 000 000 0(1)
1.0[−20]	−0.499 999 999 999 999 999 990 000 000 000	2.000 000 000 000 000 000 000 000 000 0(2)
1.0[−10]	−0.499 999 999 900 000 000 000 000 001 000	1.999 999 999 999 999 999 999 999 99(6)
1.0[−1]	−0.400 884 774 639 478 191 787 512 339 062 119	1.996 909 759 984 373 613 903 075 055 621 (3)

α	E	$C_0(0)$
0.256 302 152 411 963 526 854 820 944 383 792	$-\alpha$	1.957 912 822 160 202 047 575 184 347 065 6(3)
0.463 084 558 965 304 652 324 937 791 624 197	−1.0[−1]	1.782 252 158 449 884 757 814 245 643 159(0)
0.720 518 362 602 302 364 000 588 194 317 280	−1.0[−10]	1.472 508 433 729 934 487 578 584 22(7)[−2]
0.720 524 085 824 721 299 077 457 036 029 876	−1.0[−20]	4.656 566 841 764 155 584 5(7)[−5]
0.720 524 085 881 952 523 553 949 292 289 864	−1.0[−30]	1.472 535 729 952 123 0(5)[−7]
0.720 524 085 881 953 095 866 193 957 240 132	−1.0[−40]	4.656 566 842 627 (0)[−10]
0.720 524 085 881 953 095 871 917 079 686 781	−1.0[−50]	1.472(8)[−12]
0.720 524 085 881 953 095 871 917 136 918 005	−1.0[−60]	4.6(7)[−15]
0.720 524 085 881 953 095 871 917 136 918 576	−1.0[−65]	(4)[−16]
0.720 524 085 881 953 095 871 917 136 918 578	−1.0[−66]	(1)[−16]

Also, $Z = 1$ has been used throughout, and only the ground state is considered.

The solution is obtained from Eq. (15) by implementing the algorithm in the previous section along with our integrator discussed in [18], which is efficient for solving linear, ordinary DEs. As can be seen in Tables I–III, the screening parameter and ground state energy pair (α, E) are calculated over wide ranges, including near the critical values $\alpha \to 0^+$ and $E \to 0^-$, and the interesting intersection point where $E = -\alpha$ for the three potentials in Eq. (22).

All the calculations are done in the IEEE 754 standard quadruple precision available in modern FORTRAN for comparison purposes. The authors believe that all 33 digits reported for α and E in Tables I–III, which are very close to the

TABLE III. The calculated results of the screening parameter α, ground state energy E_0, and the value of the wavefunction at the origin C_0 for the HP potential. Values in square brackets are powers of 10. The critical value of the s states is analytically known to be $\alpha_n = 2/n^2$, $n = 1, 2, \ldots$ [20].

α	E	$C_0(0)$
1.0[−33]	−0.500 000 000 000 000 000 000 000 000 000	1.999 999 999 999 999 999 999 999 999 9(9)
1.0[−32]	−0.499 999 999 999 999 999 999 999 999 995	2.000 000 000 000 000 000 000 000 000 0(1)
1.0[−31]	−0.499 999 999 999 999 999 999 999 999 950	1.999 999 999 999 999 999 999 999 999 9(9)
1.0[−30]	−0.499 999 999 999 999 999 999 999 999 500	2.000 000 000 000 000 000 000 000 000 00
1.0[−20]	−0.499 999 999 999 999 999 995 000 000 000	2.000 000 000 000 000 000 000 000 000 0(1)
1.0[−10]	−0.499 999 999 950 000 000 001 250 000 000 000	1.999 999 999 999 999 997 500 000 00(1)
1.0[−1]	−0.451 250 000 000 000 000 000 000 000 000	1.997 498 435 543 817 891 578 038 232 806(0)
1.0	−0.125 000 000 000 000 000 000 000 000 000	1.732 050 807 568 877 293 527 446 341 505 7(0)

α	E	$C_0(0)$
0.343 145 750 507 619 804 793 245 103 161 208	$-\alpha$	1.970 342 862 018 832 077 379 003 927 623(7)
1.105 572 809 000 084 121 436 330 532 507 49	−1.0[−1]	1.666 645 962 404 632 447 695 256 364 303(4)
1.999 971 715 728 752 538 099 023 966 225 52	−1.0[−10]	1.063 644 136 976 625 377 675 776 06(7)
1.999 999 999 717 157 287 525 380 990 239 66	−1.0[−20]	3.363 585 660 539 175 326 123 (8)[−5]
1.999 999 999 999 997 171 572 875 253 809 90	−1.0[−30]	1.063 659 179 388 996 23(7)[−7]
1.999 999 999 999 999 999 971 715 728 752 54	−1.0[−40]	3.363 585 661 014 (8)[−10]
1.999 999 999 999 999 999 999 999 717 157 29	−1.0[−50]	1.06(5)[−12]
1.999 999 999 999 999 999 999 999 999 997 17	−1.0[−60]	3.3(7)[−15]
1.999 999 999 999 999 999 999 999 999 999 97	−1.0[−64]	4. (7)[−16]
1.999 999 999 999 999 999 999 999 999 999 99	−1.0[−65]	4. (5)[−16]
2.000 000 000 000 000 000 000 000 000 000 00	−1.0[−66]	1. (3)[−16]

working precision, are correct. For the upper half of the tables, α is held fixed, and E is bracketed and searched for as described in Sec. IV, and vice versa, for the bottom half, except for the case where they coincide into $E + \alpha = 0$.

One of the main results reported in this work is to show numerically what happens as one of these quantities approaches the critical value by carefully varying the parameters. For small α, all three potentials commence like a hydrogen atom, and by the time their respective eigenvalues reach $E = -\alpha$, they separate in such a way that $E(\text{HP}) < E(\text{SCP}) < E(\text{ECSCP})$, which is consistent with the findings of [20,21]. Early works [20] reported it is challenging to demonstrate the relative eigenvalues for the three potentials numerically as α gets smaller, which our work has overcome. Also proven here numerically is, $\alpha \rightarrow 0$ proportional to the change in the corresponding eigenvalue. This is in contrast to the situation near the critical value of α, where the value of E is quadratically proportional to the change in α [9,22].

However, the probability density at the origin (here C_0^2) [10], is the quantity of physical importance that we found becomes more challenging to calculate as α gets bigger. This is because the increased screening of the nucleus causes the wavefunction to spread further away from the origin, and the numerical integration over the resulting large radius becomes more time-consuming and ultimately suffers from loss of accuracy. The digits in brackets in Tables I–III indicate the first digit that changes when the order of the polynomial in our local basis set is varied by ± 1. The values of C_0 presented in the tables are accurate enough for applications done in the usual 16-digit (double) precision without any need for extrapolation.

VI. CONCLUSIONS

For all three potentials, and across a wide range, the values for the (α, E) pair are calculated close to the maximum accuracy promised by the employed working precision. The most accurate value to date is also reported for the electronic density at the origin. These results demonstrate that the DEs derived in this article and an accompanying algorithm are robust.

As it stands, it is not yet clear how Eq. (13) can be effectively used if E is unknown. While the algorithm of locating E for bound states presented in Sec. IV can easily be implemented for the one-dimensional potential $V(r)$, generally, for a potential $V(\mathbf{r})$ in higher dimensions, it does not easily translate to handle the band of orbitals ψ_L that need to be propagated together using Eq. (13). This is particularly true for bound states in atoms and molecules as the orbitals ψ_L might exponentially decay at different radii, and divergence can easily contaminate the solution with numerical overflow. This challenge remains open and a new algorithm is needed.

[1] R. G. Parr and W. Yang, *Density-Functional Theory of Atoms and Molecules*, International Series of Monographs on Chemistry (Oxford University Press, New York, 1994).

[2] A. Szabo and N. Ostlund, *Modern Quantum Chemistry: Introduction to Advanced Electronic Structure Theory* (Dover, Mineola, NY, 1996).

[3] F. W. Olver, D. W. Lozier, R. F. Boisvert, and C. W. Clark, *NIST Handbook of Mathematical Functions*, 1st ed. (Cambridge University Press, New York, NY, 2010).

[4] W. H. Press, S. A. Teukolsky, W. T. Vetterling, and B. P. Flannery, *Numerical Recipes: The Art of Scientific Computing*, 3rd ed. (Cambridge University Press, New York, NY, 2007).

[5] L. G. Jiao, L. Xu, R. Y. Zheng, A. Liu, Y. Z. Zhang, H. E. Montgomery, and Y. K. Ho, Critical screening parameters of one-electron systems with screened Coulomb potentials: High Rydberg limit, J. Phys. B: At., Mol. Opt. Phys. **55**, 195001 (2022).

[6] M. Napsuciale and S. Rodríguez, Complete analytical solution to the quantum Yukawa potential, Phys. Lett. B **816**, 136218 (2021).

[7] H. H. Xie, L. G. Jiao, A. Liu, and Y. K. Ho, High-precision calculation of relativistic corrections for hydrogen-like atoms with screened Coulomb potentials, Int. J. Quantum Chem. **121**, e26653 (2021).

[8] J. P. Edwards, U. Gerber, C. Schubert, M. A. Trejo, and A. Weber, The Yukawa potential: Ground state energy and critical screening, Prog. Theor. Exp. Phys. **2017**, 083A01 (2017).

[9] L. G. Jiao, H. H. Xie, A. Liu, H. E. Montgomery, and Y. K. Ho, Critical screening parameters and critical behaviors of one-electron systems with screened Coulomb potentials, J. Phys. B: At., Mol. Opt. Phys. **54**, 175002 (2021).

[10] X. H. Ji, Y. Y. He, L. G. Jiao, A. Liu, and Y. K. Ho, Probability density of the Yukawa particle at the origin: Numerical calculation and analytical solution, Phys. Lett. B **823**, 136718 (2021).

[11] J. D. Jackson, *Classical Electrodynamics*, 3rd ed. (Wiley, New York, NY, 1999), Chap. 1, p. 35.

[12] D. Gebremedhin and C. Weatherford, *Hartree-Fock Calculations on Atoms with Coulomb Sturmian Basis Sets* (Academic, New York, 2023), Chap. 7, pp. 119–132.

[13] S. Hassani, *Mathematical Physics: A Modern Introduction to Its Foundations* (Springer, Cham, 2013), Chap. 6, pp. 178–179.

[14] E. Hairer, S. P. Nørsett, and G. Wanner, *Solving Ordinary Differential Equations I: Nonstiff Problems,* 2nd revised. ed. (Springer-Verlag, Berlin, Heidelberg, 1993).

[15] G. Rawitscher, Tunneling through a barrier with the phase–amplitude method, Comput. Phys. Commun. **203**, 138 (2016).

[16] S. Kiyokawa, Exact solution to the Coulomb wave using the linearized phase-amplitude method, AIP Adv. **5**, 087150 (2015).

[17] U. Peskin, *Quantum Mechanics in Nanoscience and Engineering* (Cambridge University Press, Cambridge, UK, 2023), Chap. 2, pp. 5–9.

[18] D. H. Gebremedhin and C. A. Weatherford, Calculations for the one-dimensional soft Coulomb problem and the hard Coulomb limit, Phys. Rev. E **89**, 053319 (2014).

[19] W. Johnson, *Atomic Structure Theory: Lectures on Atomic Physics* (Springer-Verlag, Berlin, Heidelberg, 2007), Chap. 2, pp. 41–45.

[20] C. Stubbins, Bound states of the Hulthén and Yukawa potentials, Phys. Rev. A **48**, 220 (1993).

[21] X. R. Wang, General theorem on the Schrödinger equation, Phys. Rev. A **46**, 7295 (1992).

[22] M. Klaus and B. Simon, Coupling constant thresholds in nonrelativistic quantum mechanics. I. Short-range two-body case, Ann. Phys. **130**, 251 (1980).

Correction: The expression for the HP potential in Eq. (22) contained minor errors and has been fixed.